A Appendix

A.1 Algorithm for the Proposed Message Passing

Algorithm 1 The Proposed Message Passing

for $i = 1, ..., n$ **do**
  for $j = 1, ..., k$ **do**
    Compute $d_{ij} = ||\mathbf{p}_i - \mathbf{p}_j||_2$
  end for
  Get reference nodes via

$$f_i = \text{argmin}_{k \in \mathcal{N}_i}(d_{ik}), s_i = \text{argmin}_{k \in \mathcal{N}_i \setminus \{f_i\}}(d_{ik})$$

end for
for $i = 1, ..., n$ **do**
  for $j = 1, ..., k$ **do**
    Get reference nodes via

$$f_{i\setminus j} = \begin{cases} f_i, & \text{if } f_i \neq j \\ s_i, & \text{otherwise} \end{cases}, f_{j\setminus i} = \begin{cases} f_j, & \text{if } f_j \neq i \\ s_j, & \text{otherwise} \end{cases}$$

    Compute angles via

$$\begin{aligned} \theta_{ij} &= \text{angle}_1(f_i, i, j), \\ \phi_{ij} &= \text{angle}_2(\text{plane}_{f_i,i,s_i}, \text{plane}_{f_i,i,j}), \\ \tau_{ij} &= \text{angle}_3(\text{plane}_{f_{i\setminus j},i,j}, \text{plane}_{i,j,f_{j\setminus i}}), \end{aligned}$$

  end for
  Update node features via Eq. 1
end for

As rigorously shown in Algorithm 1 , there are two nested loops in the message passing. For each nested loop, the complexity for the outer loop is $O(n)$, and the complexity for the inner loop is $O(k)$. Particularly, within the inner loop, the operations are picking proper reference nodes, thus the complexity is simply $O(1)$. Overall, the total complexity of our message passing is $O(nk)$. Importantly, the efficiency of our method is also demonstrated in Sec. 6 that ComeNet is 6-10 times faster than SphereNet. Actually, the training time of ComENet is similar to SchNet whose complexity is also $O(nk)$.

A.2 SE(3)

SE(3) is the Special Euclidean group in 3 dimensions, including all rotations and translations in 3D. It is the set of 4×4 real matrices of the form

$$\begin{bmatrix} Rot & \mathbf{t} \\ 0 & 1 \end{bmatrix} = \begin{bmatrix} r_{11} & r_{12} & r_{13} & t_1 \\ r_{21} & r_{22} & r_{23} & t_2 \\ r_{31} & r_{32} & r_{33} & t_3 \\ 0 & 0 & 0 & 1 \end{bmatrix}, \tag{1}$$

where $Rot \in \text{SO}(3)$ and $\mathbf{t} \in \mathbb{R}^3$. The SO(3) is the set of 3×3 real matrices Rot satisfying $Rot^T Rot = I$ and $\det(Rot) = 1$.

A.3 Proofs of Lemma 1

Proof. We employ contradiction to prove it. Basically, there exist two cases when adding this new node j, as illustrated in Fig. 1 and described as following. *Case (1): i has more than one neighboring nodes $c_{1,2,...}$; Case (2): i only has one neighboring node c_1.*

Generally, in case (1), we need to prove $\mathbf{p}_{ij}$ is uniquely defined as $(d_{ij}, \theta_{ij}, \phi_{ij})$; in case (2), we need to prove $\mathbf{p}_{ij}$ is uniquely defined as $(d_{ij}, \theta_{ij}, \tau_{c_1 i})$. We assume there exists another location for j such that there is a different relative location vector $\widetilde{\mathbf{p}}_{ij}$, and this assumption leads to contradiction. The proofs of both cases are provided below. □

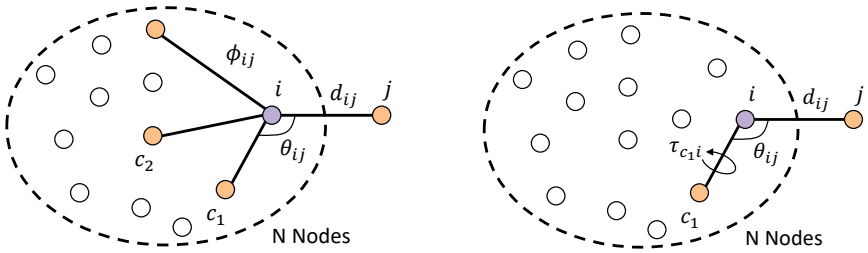

Case (1): i has more than one neighboring nodes $c_{1,2,...}$

Case (2): i only has one neighboring node c_1

Figure 1: Two cases for proving Lemma 1 when generalizing the size of a 3D graph from k to $k+1$.

Proof of case (1): In case (1), we need to prove $\mathbf{p}_{ij}$ is uniquely defined as $(d_{ij}, \theta_{ij}, \phi_{ij})$. Based on the notations defined in Sec. 2.4, we have

$$\begin{aligned} \langle \mathbf{p}_{ij}, \mathbf{p}_{ij} \rangle &= d_{ij}^2, \\ \langle \mathbf{p}_{if_i}, \mathbf{p}_{ij} \rangle &= d_{if_i} d_{ij} cos\theta_{ij}, \\ \langle T(\mathbf{p}_{is_i}), T(\mathbf{p}_{ij}) \rangle &= \|T(\mathbf{p}_{is_i})\| \|T(\mathbf{p}_{ij})\| cos\phi_{ij}, \\ \langle T(\mathbf{p}_{is_i}) \times T(\mathbf{p}_{ij}), \mathbf{p}_{if_i} \rangle &= d_{if_i} \|T(\mathbf{p}_{is_i})\| \|T(\mathbf{p}_{ij})\| sin\phi_{ij}, \end{aligned} \tag{2}$$

where T denotes an operator of projection to the plane perpendicular to $\mathbf{p}_{if_i}$. Apparently, all the quantities on the right side are known based on Sec. 2.4. Assume the solution set contains at least two different solutions $\mathbf{p}_{ij}$ and $\widetilde{\mathbf{p}}_{ij}$. Eq. 2 can simply imply that

$$\begin{aligned} \langle \mathbf{p}_{if_i}, \mathbf{p}_{ij} - \widetilde{\mathbf{p}}_{ij} \rangle &= 0, \\ \langle T(\mathbf{p}_{is_i}), \mathbf{p}_{ij} - \widetilde{\mathbf{p}}_{ij} \rangle &= 0, \\ \langle T(\mathbf{p}_{is_i}) \times (\mathbf{p}_{ij} - \widetilde{\mathbf{p}}_{ij}), \mathbf{p}_{if_i} \rangle &= 0. \end{aligned} \tag{3}$$

Apparently, both $T(\mathbf{p}_{is_i})$ and $\mathbf{p}_{ij} - \widetilde{\mathbf{p}}_{ij}$ are in the plane perpendicular to $\mathbf{p}_{if_i}$. Hence, $T(\mathbf{p}_{is_i}) \times (\mathbf{p}_{ij} - \widetilde{\mathbf{p}}_{ij}) = \alpha \mathbf{p}_{if_i}$ holds for some $\alpha \neq 0$. However, from Eq. 3, we have

$$\langle T(\mathbf{p}_{is_i}) \times (\mathbf{p}_{ij} - \widetilde{\mathbf{p}}_{ij}), \mathbf{p}_{if_i} \rangle = \alpha \langle \mathbf{p}_{if_i}, \mathbf{p}_{if_i} \rangle = 0. \tag{4}$$

Since $\alpha \neq 0$ and $\mathbf{p}_{if_i} \neq \mathbf{0}$, Eq. 4 causes a contradiction. Thus, the solution set contains a unique solution.

Proof of case (2): In case (2), we need to prove $\mathbf{p}_{ij}$ is uniquely defined by $(d_{ij}, \theta_{ij}, \tau_{c_1 i})$. Based on the notations defined in Sec. 2.4 and Sec. 2.2, we have

$$\begin{aligned} \langle \mathbf{p}_{ij}, \mathbf{p}_{ij} \rangle &= d_{ij}^2, \\ \langle \mathbf{p}_{if_i}, \mathbf{p}_{ij} \rangle &= d_{if_i} d_{ij} cos\theta_{ij}, \\ \left\langle T(\mathbf{p}_{if_{if_{i\setminus i}}}), T(\mathbf{p}_{ij}) \right\rangle &= \|T(\mathbf{p}_{if_{if_{i\setminus i}}})\| \|T(\mathbf{p}_{ij})\| cos\tau_{c_1 i}, \\ \left\langle T(\mathbf{p}_{if_{if_{i\setminus i}}}) \times T(\mathbf{p}_{ij}), \mathbf{p}_{if_i} \right\rangle &= d_{if_i} \|T(\mathbf{p}_{if_{if_{i\setminus i}}})\| \|T(\mathbf{p}_{ij})\| sin\tau_{c_1 i}, \end{aligned} \tag{5}$$

where T still denotes an operator of projection to the plane perpendicular to $\mathbf{p}_{if_i}$. Similarly, all the quantities on the right side are known based on Sec. 2.4 and Sec. 2.2. Assume the solution set

contains at least two different solutions $\mathbf{p}_{ij}$ and $\widetilde{\mathbf{p}}_{ij}$. Eq. 5 can simply imply that

$$\begin{aligned} \left\langle \mathbf{p}_{if_i}, \mathbf{p}_{ij} - \widetilde{\mathbf{p}}_{ij} \right\rangle &= 0, \\ \left\langle T(\mathbf{p}_{f_i f_{f_i \setminus i}}), \mathbf{p}_{ij} - \widetilde{\mathbf{p}}_{ij} \right\rangle &= 0, \\ \left\langle T(\mathbf{p}_{f_i f_{f_i \setminus i}}) \times (\mathbf{p}_{ij} - \widetilde{\mathbf{p}}_{ij}), \mathbf{p}_{if_i} \right\rangle &= 0. \end{aligned} \tag{6}$$

Both $T(\mathbf{p}_{f_i f_{f_i \setminus i}})$ and $\mathbf{p}_{ij} - \widetilde{\mathbf{p}}_{ij}$ are in the plane perpendicular to $\mathbf{p}_{if_i}$. Hence, $T(\mathbf{p}_{f_i f_{f_i \setminus i}}) \times (\mathbf{p}_{ij} - \widetilde{\mathbf{p}}_{ij}) = \alpha \mathbf{p}_{if_i}$ holds for some $\alpha \neq 0$. However, from Eq. 6, we have

$$\left\langle T(\mathbf{p}_{f_i f_{f_i \setminus i}}) \times (\mathbf{p}_{ij} - \widetilde{\mathbf{p}}_{ij}), \mathbf{p}_{if_i} \right\rangle = \alpha \left\langle \mathbf{p}_{if_i}, \mathbf{p}_{if_i} \right\rangle = 0. \tag{7}$$

Since $\alpha \neq 0$ and $\mathbf{p}_{if_i} \neq \mathbf{0}$, Eq. 7 causes a contradiction. Thus, the solution set contains a unique solution.

A.4 Model architecture

Interaction Layer updates each node feature vector $\mathbf{v}$ based on features of the neighboring nodes and the corresponding 3D information in P. Firstly, it converts 3D information in P to a set of geometries based on the proposed complete geometric transformation $\mathcal{T}$ and message passing scheme. Since distance is the most important geometry, we also consider d in global representation and split the output of $\mathcal{T}$ into two tuples (d, θ, ϕ) and (d, τ), for local and global representations, respectively.

Importantly, the tuples (d, θ, ϕ) and (d, τ) cannot serve as immediate inputs to the network. They need to be transformed into physically meaningful vectors based on quantum-based basis functions. As in previous studies [6, 3, 8, 4], we test different basis functions including MLP, Gaussian and sine functions, spherical Bessel functions, and spherical harmonics. We found spherical Bessel and spherical harmonics perform best. Formally, the basis function for tuple (d, θ, ϕ) is TBF $j_\ell \left(\frac{\beta_{\ell n}}{c} d \right) Y_\ell^m(\theta, \phi)$, where $j_\ell(\cdot)$ is a spherical Bessel function of order ℓ, Y_ℓ^m is a spherical harmonic function of degree m and order ℓ, c is the cutoff, and $\beta_{\ell n}$ is the n-th root of the Bessel function of order ℓ. The basis function for tuple (d, τ) is SBF $j_\ell \left(\frac{\beta_{\ell n}}{c} d \right) Y_\ell^0(\tau)$. These two basis functions are also used in SphereNet [8] and GemNet [4].

The two physically meaningful vectors from TBF and SBF are then imported into a local convolution layer and a global convolution layer, respectively. For both convolution layers, we use the GraphConv [9] implemented in the PyTorch Geometric library [2]. The vectors from the basis functions are used as edge weights in the convolution layers. The outputs of local and global convolution layers are concatenated to generate a new node feature vector. Then the concatenated vector is forwarded into several linear layers to generate the updated feature vector $\mathbf{v}'$.

A.5 Data Description

OC20. The Open Catalyst 2020 (OC20) dataset [1] is a newly released dataset to model and discover catalysts. Specifically, the goal is efficient DFT approximation of structure relaxation, which is a fundamental calculation in catalysis to determine a structure's activity and selectivity. All the structures in the dataset contain a surface and an adsorbate, and the surface is defined by a unit cell that is periodic in all directions. There are three tasks including Structure to Energy and Forces (S2EF), Initial Structure to Relaxed Structure (IS2RS), and Initial Structure to Relaxed Energy (IS2RE).

In this work, we focus on Initial Structure to Relaxed Energy (IS2RE) task, which is the most common task in catalysis as the relaxed energies are often correlated with catalyst activity and selectivity. The dataset for IS2RE is originally split into training, validation, and test sets. The training set contains 460,328 structures and the validation set has four splits including in-domain (ID), out-of-domain adsorbate (OOD Ads), out-of-domain catalyst (OOD Cat), and out-of-domain adsorbate and catalyst (OOD Both), with 24,733, 24,961, 24,738, 24,971 structures respectively.

Molecule3D. The Molecule3D dataset [13] is a newly proposed large-scale dataset, including around 4 million molecules with precise ground-state geometries derived from DFT. The dataset is collected from PubChemQC [10] and designed for predicting 3D geometries from molecular graphs [13] while we aim to learn representations and predict properties for molecules based on their geometries. The dataset contains 3,899,647 molecules and is split into training, validation, and test sets via random and scaffold split with ratio 6:2:2. Random split ensures the training, validation, and test data are sampled from the same distribution while scaffold split leads to a distribution shift between training and test data. The evaluation metric is the MAE between the predictions and the ground truth.

QM9. The QM9 dataset [11] is a widely used dataset for predicting various properties of molecules. It includes geometric, energetic, electronic, and thermodynamic properties for 134k stable small organic molecules. The dataset is split into three sets, where the training set contains 110,000, the validation set contains 10,000, and the test set contains 10,831 molecules. The twelve properties are dipole moment (μ), isotropic polarizability (α), highest occupied molecular orbital energy (ϵ_{HOMO}), lowest unoccupied molecular orbital energy (ϵ_{LUMO}), gap between ϵ_{HOMO} and ϵ_{LUMO}, electronic spatial extent ($\langle R^2 \rangle$), zero point vibrational energy (ZPVE), internal energy at 0K (U_0), internal energy at 298.15K (U) , enthalpy at 298.15K (H), free energy at 298.15K (G) , and heat capavity at 298.15K (c_{v}).

A.6 Experimental Setup

ComENet. The values/search space of model and training hyperparameters for ComENet on OC20, Molecule3D, and QM9 are provided in Table 1 and Table 2. For Molecule3D and QM9, the optimal hyperparameters are chosen by the performance on the validation sets. For OC20, since the final comparison results are on validation set, we firstly use 10% of the training data to choose optimal hyperparameters, then train our model on whole training data. Specifically, we use a larger cutoff value for OC20 to generate graphs and larger hidden dimensions for OC20 and Molecule3D. All models are trained on NVIDIA GeForce RTX 2080 Ti 11GB GPU for Molecule3D and QM9. For the OC20 dataset, we use NVIDIA RTX A6000 48GB GPU. Note that one experiment is only conducted on one GPU.

Baselines for Molecule3D. As Molecule3D is a newly proposed dataset, we run experiments and provide results for baseline methods including GIN-Virtual [5], SchNet [12], DimeNet++[7] and SphereNet [8]. All the models are trained on one GPU (Nvidia GeForce RTX 2080 Ti 11GB). The model hyperparameters and training hyperparameters are listed in Table 3 and Table 4. The optimal hyperparameters are chosen by the performance on validation set. Note that for DimeNet++[7] and SphereNet [8], the maximum batch size is 32 due to the GPU memory limitation.

Table 1: Model hyperparameters for ComENet.

	Values/ search space		
Model Hyperparameters	OC20	Molecule3D	QM9
Number of layers	4, 5, 6	4, 5, 6, 8	4, 5, 6
Cutoff	6.0, 8.0	5.0	5.0
Hidden dim	128, 256, 512	128, 256, 512	128, 256
Hidden dim in Self-Atom layer	128, 256, 512	128, 256, 512	128, 256
Number of layers in Self-Atom layer	2, 3, 4	2, 3, 4	2, 3, 4
Number of layers of the MLP in Interaction layer	2, 3, 4	2, 3, 4	2, 3, 4
Distance embedding dim	6, 12	6, 12	6, 12
Angle embedding dim	3, 6	3, 6	3, 6

Table 2: Training hyperparameters for ComENet.

Training hyperparameters	Values/ search space		
	OC20	Molecule3D	QM9
Epochs	20	300	1000
Batch size	64, 128	128, 256	32, 64, 128
Learning rate 1e-3, 5e-4, 2e-4	1e-3, 5e-4, 2e-4	1e-3, 5e-4, 2e-4	1e-3, 5e-4, 2e-4
Learning rate decay factor	0.4, 0.5, 0.6	0.4, 0.5, 0.6	0.4, 0.5, 0.6
Learning rate decay epochs	Milestone [4,7,10,12]	20, 30, 50	100, 200
Warmup epochs	2	–	–
Warmup factor	0.2	–	–

Table 3: Model hyperparameters for baseline methods on Molecule3D.

Model Hyperparameters	Values/ search space			
	GIN-Virtual	SchNet	DimeNet++	SphereNet
Number of layers	4, 6, 8	4, 6, 8	3, 4, 5, 6	3, 4, 5, 6
Cutoff	-	10.0	6.0	6.0
Hidden dim	600	256	128	128

Table 4: Training hyperparameters for baseline methods on Molecule3D.

Training hyperparameters	Values/ search space			
	GIN-Virtual	SchNet	DimeNet++	SphereNet
Epochs	300	300	300	300
Batch size	64, 128, 256	64, 128, 256	16, 32	16, 32
Learning rate	1e-3, 5e-4, 2e-4	1e-3, 5e-4, 2e-4	1e-3, 5e-4, 2e-4	1e-3, 5e-4, 2e-4
Learning rate decay factor	0.4, 0.5, 0.6	0.4, 0.5, 0.6	0.4, 0.5, 0.6	0.4, 0.5, 0.6
Learning rate decay epochs	20, 30, 50	20, 30, 50	20, 30, 50	20, 30, 50

References

[1] Lowik Chanussot, Abhishek Das, Siddharth Goyal, Thibaut Lavril, Muhammed Shuaibi, Morgane Riviere, Kevin Tran, Javier Heras-Domingo, Caleb Ho, Weihua Hu, et al. Open catalyst 2020 (OC20) dataset and community challenges. *ACS Catalysis*, 11(10):6059–6072, 2021.

[2] Matthias Fey and Jan E. Lenssen. Fast graph representation learning with PyTorch Geometric. In *ICLR Workshop on Representation Learning on Graphs and Manifolds*, 2019.

[3] Johannes Gasteiger, Janek Groß, and Stephan Günnemann. Directional message passing for molecular graphs. In *International Conference on Learning Representations*, 2020. URL https://openreview.net/forum?id=B1eWbxStPH.

[4] Johannes Gasteiger, Florian Becker, and Stephan Günnemann. Gemnet: Universal directional graph neural networks for molecules. *Advances in Neural Information Processing Systems*, 34: 6790–6802, 2021.

[5] Weihua Hu, Matthias Fey, Hongyu Ren, Maho Nakata, Yuxiao Dong, and Jure Leskovec. OGB-LSC: A large-scale challenge for machine learning on graphs. In *Thirty-fifth Conference on Neural Information Processing Systems Datasets and Benchmarks Track (Round 2)*, 2021. URL https://openreview.net/forum?id=qkcLxoC52kL.

[6] Weihua Hu, Muhammed Shuaibi, Abhishek Das, Siddharth Goyal, Anuroop Sriram, Jure Leskovec, Devi Parikh, and C Lawrence Zitnick. ForceNet: A graph neural network for large-scale quantum calculations. *arXiv preprint arXiv:2103.01436*, 2021.

[7] Johannes Klicpera, Shankari Giri, Johannes T Margraf, and Stephan Günnemann. Fast and uncertainty-aware directional message passing for non-equilibrium molecules. In *NeurIPS-W*, 2020.

[8] Yi Liu, Limei Wang, Meng Liu, Yuchao Lin, Xuan Zhang, Bora Oztekin, and Shuiwang Ji. Spherical message passing for 3D molecular graphs. In *International Conference on Learning Representations*, 2022. URL https://openreview.net/forum?id=givsRXsOt9r.

[9] Christopher Morris, Martin Ritzert, Matthias Fey, William L Hamilton, Jan Eric Lenssen, Gaurav Rattan, and Martin Grohe. Weisfeiler and leman go neural: Higher-order graph neural networks. In *Proceedings of the AAAI Conference on Artificial Intelligence*, volume 33, pages 4602–4609, 2019.

[10] Maho Nakata and Tomomi Shimazaki. PubChemQC project: a large-scale first-principles electronic structure database for data-driven chemistry. *Journal of chemical information and modeling*, 57(6):1300–1308, 2017.

[11] Raghunathan Ramakrishnan, Pavlo O Dral, Matthias Rupp, and O Anatole Von Lilienfeld. Quantum chemistry structures and properties of 134 kilo molecules. *Scientific data*, 1(1):1–7, 2014.

[12] Kristof Schütt, Pieter-Jan Kindermans, Huziel Enoc Sauceda Felix, Stefan Chmiela, Alexandre Tkatchenko, and Klaus-Robert Müller. SchNet: A continuous-filter convolutional neural network for modeling quantum interactions. In *Advances in Neural Information Processing Systems*, pages 991–1001, 2017.

[13] Zhao Xu, Youzhi Luo, Xuan Zhang, Xinyi Xu, Yaochen Xie, Meng Liu, Kaleb Dickerson, Cheng Deng, Maho Nakata, and Shuiwang Ji. Molecule3D: A benchmark for predicting 3D geometries from molecular graphs. *arXiv preprint arXiv:2110.01717*, 2021.